Journal of Materials Chemistry C

Accepted Manuscript

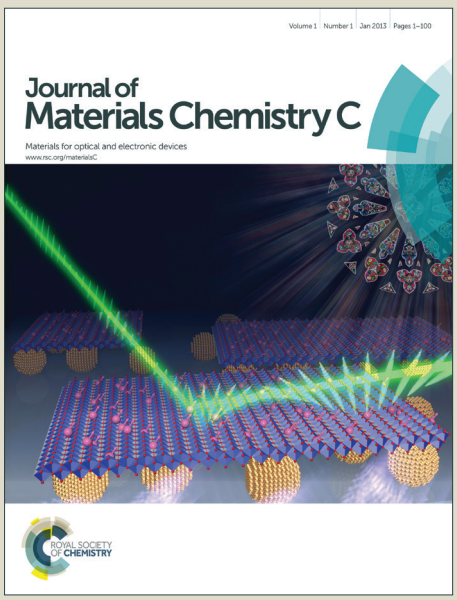

ROYAL SOCIETY OF CHEMISTRY

www.rsc.org/materialsC

Journal of
Materials Chemistry C

RSCPublishing

ARTICLE

Novel Dithiols as Capping Ligands for CdSe Quantum Dots: Optical Properties and Solar Cell Applications†

Cite this: DOI: 10.1039/x0xx00000x

Avvaru Praveen Kumar,[a] Bui The Huy,[a,b] Begari Prem Kumar,[a] Jong Hwa Kim,[a] Van-Duong Dao,[c] Ho-Suk Choi[c] and Yong-Ill Lee[a*]

Received 00th January 2014,
Accepted 00th January 2014

DOI: 10.1039/x0xx00000x

www.rsc.org/

Recently, organic ligands have been shown to play a significant role in optical, electronic properties and also solar cell applications. We report organic dithiols as novel capping ligands for CdSe quantum dots (QDs). The organic dithiol compounds were designed in such a way that the two thiols groups of a dithiol (acts as bidentate ligand) can bond directly to inorganic CdSe QD surface which passivate effectively to show high optical efficiency by promoting interfacial charge transfer. This work would offer a direct and effective pathway to synthesize CdSe QDs that attaches dithiol ligands with aromatic functionality while maintaining the size and shape control of the CdSe QDs. The structure, crystallinity, and optical property of the dithiol-capped CdSe QDs were analyzed by XRD, TEM, and photoluminescence. The covalent immobilization of dithiols onto CdSe QDs was confirmed by XPS, FT-IR, TGA, XRD and TEM characterizations. Further, the influence of dithiol-type capping ligands on the optical properties of highly luminescent CdSe QDs was investigated. It has been found that the growth rate and photoluminescence intensity of CdSe QDs were strongly dependent on the type of dithiol ligands. We also experimentally investigated the use of dithiol-capped CdSe QDs in solar cells. The dithiol shell allows for the electron transport from the surface of the QDs, evidenced by better performance as CdSe QDs sensitized solar cells. The power conversion efficiency (η) of CdSe QDs reached up to 0.65%.

Introduction

Among II–VI semiconductor compounds, CdSe has attracted much interest because of its comparatively easy synthesis and its direct optical band gap energy of 1.74 eV, which facilitates emission in the visible spectral range through size control due to quantum confinement of charge carriers. Due to its outstanding structural and optical properties and good chemical and mechanical stability, CdSe is well suited for application in optoelectrical devices such as light amplifiers, light-emitting diodes, thin film transistors, single electron transistors, lasers, solar energy conversion devices, and biomedical imaging agents.[1-5]

Quantum-dot-sensitized solar cells (QDSSCs) are important materials in new generation photovoltaic devices[6, 7] because of the ability to tune their semiconductor band gaps, their high extinction coefficients, large molecular dipoles, and potential multilayer sensitization.[8-11] Among the different types of QDs, CdSe are the first nanocrystal (NC) QDs to be employed in solar cells. CdSe QDs have several advantages; synthetic methods to produce CdSe QDs are well developed, they absorb light at a suitable spectral range (from 300 to 650 nm) for harvesting solar emission, and they are good electron acceptors.[12] Further, they exhibit higher power conversion efficiency (PCE) than solar cell devices incorporating QDs made from other materials,[13, 14]and are under investigation for utilization in hybrid solar cells.[15]

QDs are capped with ligands that can be inorganic, organic, or polymer-type; these capping ligands are necessary for their solution-based synthesis and also pertinent to their chemical processability, which is a key advantage in device production and also improves photoluminescence (PL). Inorganic QDs have been capped with organic ligands such as trioctylphosphine oxide,[16] oleic acid,[17] pyridine,[18] thiols[19, 20] and amines[21]; however, most of these capping ligands preclude electron transfer transport and therefore function as insulators. To overcome this problem, three methods have been utilized:[22] (i) preparation of organic ligand-capped inorganic QDs in which organic ligands are thermally cleavable,[23] (ii) ligand exchange, which involves the exchange of the original organic ligand for another organic ligand,[16, 17, 24, 25] and (iii) direct synthesis of hybrid inorganic NCs capped with organic ligands. However, the first method requires thermally cleavable organic ligands, and there are few thermally cleavable solubilizing ligands. The second ligand exchange method involves lengthy, costly, and complicated experimental procedures, and also complete ligand exchange is difficult, which would be reflected in variations in optical and other

[a]*Department of Chemistry, Changwon National University, Changwon 641-773, Korea.*
E-mail: yilee@changwon.ac.kr; Fax: +82-55-213-3439; Tel: +82-55-213-3436
[b]*Nhatrang Institute of Technology Research and Application, Vietnam Academy of Science and Technology (VAST), 2 Hung Vuong, Nhatrang, Vietnam.*
[c]*Department of Chemical Engineering, Chungnam National University, Daejeon, Korea.*

†Electronic Supplementary Information (ESI) Available: Synthesis of dithiols; FT-IR spectra; TGA curves; comparison of PL intensities; photocurrent density-voltage curve.

properties. The last method, direct synthesis of ligand-capped inorganic QDs, overcomes the limitations of the other two methods. We therefore directly synthesized organic ligand-capped CdSe QDs.

Some studies have shown that organic ligands can make significant contributions to the optical and electronic properties of QDs[25-28] as well as solar cells.[29, 30] The search for novel organic ligands for CdSe semiconductor QDs to provide them with useful functionalities is an active research area. The electron transfer at the interface between inorganic and organic materials in organic ligand-capped inorganic QDs needs improvement. Inorganic NCs possess higher electron affinities, which make them energetically favorable for electron transport onto the organic ligand layer. Here, we chose dithiols (DTs) (ESI Scheme S1†) as new ligands to effectively passivate the CdSe surface to improve optical efficiency. We reasoned that the two thiols groups of a DT molecule bonded to an inorganic CdSe QD surface would offer a direct path to synthesize DT-capped CdSe QDs for highly effective passivation, rather than requiring the exchange of the original organic ligand for another organic ligand. To the best of our knowledge, no previous study has reported the synthesis of new DTs (ESI Scheme S1†) or DT-capped CdSe QDs for solar cell applications.

Results and Discussion

Scheme 1 shows the mechanism of capping of CdSe quantum dots with organic DTs (A-D). Synthesis of organic DTs ligands was simple and their successful formation was confirmed by ^{1}H- and ^{13}C-NMR, FT-IR, and ESI-MS techniques. We designed organic DT ligands for the following three reasons: (i) DTs consist of two –SH groups, and therefore act as bidentate ligands (anchoring sites), which should allow them to co-ordinate more strongly with the CdSe QD surface due to the presence of multiple binding sites,[31-34] (ii) stronger coordination of DTs with CdSe QDs could enhance optical properties, and (iii) DT ligands could potentially facilitate charge transfer. We confirmed the surface modification of CdSe QDs with DTs by XPS, FT-IR, TGA, XRD, and TEM characterizations.

XPS characterization is widely used to identify the chemical environment of an atom and the electronic structure of a material because it provides the binding energy of a core-level electron of an atom in the solid. Binding energy depends on the potential energy at that position, which in turn depends on the chemical environment of the atom.[35] XPS spectra of DT-capped-CdSe QDs revealed the existence of cadmium, selenium, carbon, sulfur, and nitrogen species in all QD samples.

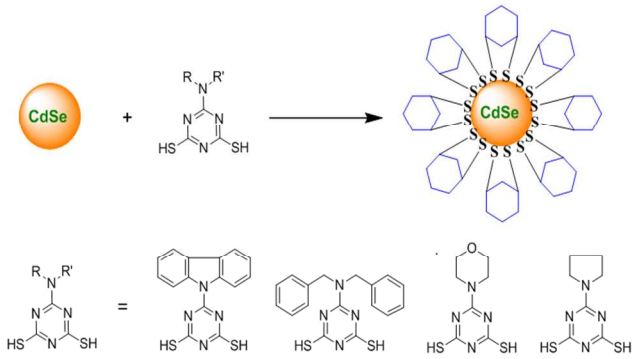

Scheme 1. Mechanism of capping of CdSe QD surfaces with dithiols.

High-resolution XPS spectra of DT-capped-CdSe QDs are shown in Fig. 1. Two strong peaks corresponding to Cd were detected in all DT-capped CdSe QDs; one was in the range of 405 - 406 eV, and the other in the range of 412 - 412.5 eV (Fig. 1a). These two peaks are related to the Cd3d5/2 and Cd3d3/2 binding energies. The appearance of a characteristic selenium XPS peak (Fig. 1b), Se3d, was observed between 54.5 - 55 eV. Binding energies of Cd3d5/2, Cd3d3/2, as well as Se3d core-levels matched those in bulk CdSe.[36-38] The spectra were in good agreement with XPS spectra reported in previous studies.[36, 38, 39] We ascribed shifts in the binding energies of Cd3d5/2 and Se3d core-levels compared to standard values to the

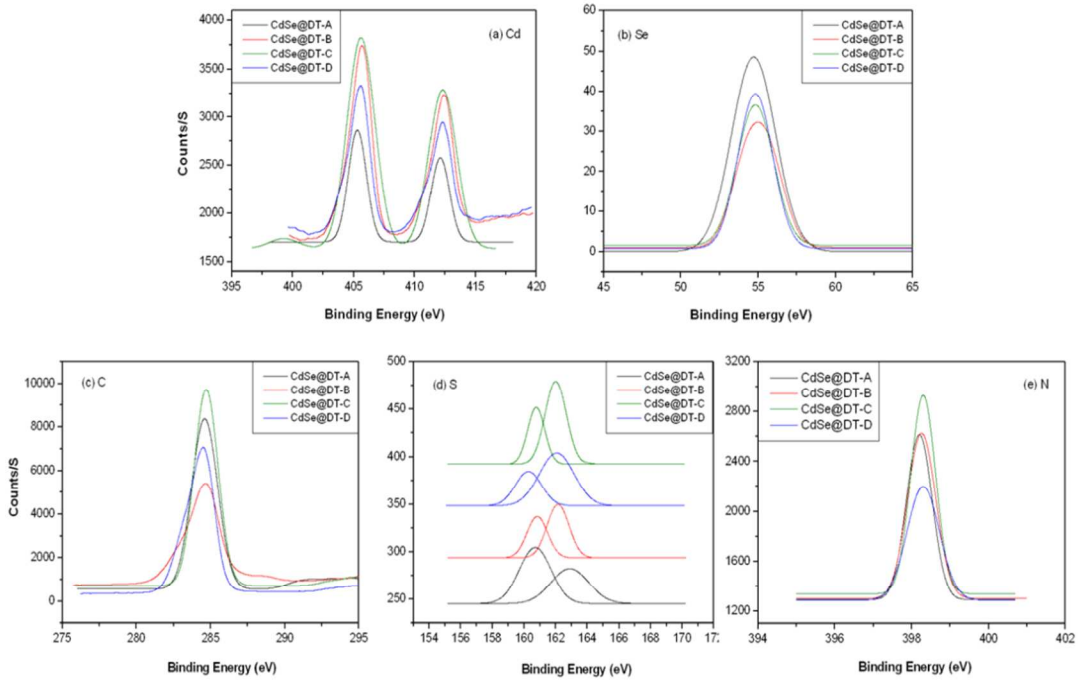

Figure 1. High-resolution XPS spectra of DT-capped CdSe QDs.

presence of bonded DTs. The intensity of Cd3d5/2 and Se3d peaks varied with different DTs, indicating that the shifts were not cause by surface oxidation but by stronger bonding of the CdSe QDs. To confirm the binding of DT ligands to the CdSe surface, high-resolution XPS spectra of carbon, sulphur, and nitrogen atoms were obtained. C 1s peak position of the carbon atoms of DTs was found at 284.5 eV (Fig. 1c). Sulfur content in the XPS spectrum (Fig. 1d) was reflected by S 2s and S 2p peaks centered at 160.2–160.7 and 162–163 eV, respectively. Nitrogen atom was assigned as N 1s and identified at 398.3 eV (Fig. 1e). These results indicate that all DTs were successfully bonded to the surfaces of CdSe QDs.

FT-IR spectra of DT-capped CdSe QDs are shown in ESI Fig. S2†. All DT-capped CdSe QD samples showed a characteristic aromatic stretching frequency between 2950-2850 cm^{-1}, aromatic C=C bending between 1530-1450 cm^{-1}, and a C-N peak between 1150-1240 cm^{-1}. Furthermore, the -SH stretching vibration located in the range of 2565-2575 cm^{-1} was not detected in the DT-capped CdSe QDs, which suggested that the S-H bonds broke and that the sulfur bonded to Cd.[39] To estimate the thermal stability of DT-capped CdSe QDs, we performed TGA measurements in a N_2 environment. TGA curves of CdSe and DT-capped CdSe QDs are presented in ESI Fig. S3†. For comparison, the TGA curve of the CdSe QD sample (ESI Fig. S3†) was also recorded. Initial decomposition occurred at around 250°C and a total weight loss of 85% occurred up to 650°C. The TGA curves of all DT-capped CdSe QDs, except for DT-A-capped CdSe QDs, showed an initial weight loss at 175°C and 15-18% weight loss between 175-370°C due to bonded organic content from DTs. Due to the high melting point of DT-A, weight loss in the CdSe-capped DT-A sample only started at 290°C. Decomposition temperature of DT-capped CdSe QDs was higher than that of pristine CdSe QDs, indicating the formation of strong bonding between CdSe and the sulfur groups of DT ligands. Further, weight loss of the A and B DT-capped CdSe QD samples was 60%, while that of the C and D DT-capped CdSe QD samples was 50%, suggesting strong and stable bonding of DTs to the CdSe surface as reflected by the higher thermal stabilities of DT-capped CdSe QDs than pristine CdSe QDs. Weight loss of DT-capped CdSe QDs was less than that of pristine CdSe QDs, suggesting that a large amount of DTs were bonded to the CdSe surface.

XRD spectra of DT-capped CdSe QDs were characterized by broad peaks, indicating the formation of small NCs. XRD patterns of pristine CdSe and DT-capped CdSe QDs are shown in Fig. 2. All diffraction peaks of pristine CdSe and DT-capped CdSe QDs were cubic (zinc blende phase) structures, as was the case for pristine CdSe. These peaks were located at angles (2θ) of 25.36°, 42.02°, and 49.72° corresponding to reflection from the (1 1 1), (2 2 0), and (3 1 1) crystal planes, respectively, (JCPDS No. 88-2346). Diffraction peaks of DT-capped CdSe QDs shifted to higher angles and were broader than those of pristine CdSe. DT-capped CdSe QDs had a cubic structure with three diffraction peaks located between those of cubic CdSe (JCPDS No. 88-2346) and CdS (JCPDS No. 89-0440). When DTs were used as stabilizers, the –SH group of DT broke and sulfur was incorporated into the crude CdSe QD crystal lattice, resulting in formation of a CdSe(S) structure.[40, 41] We calculated that the grain size of QDs was 4 nm using the Scherrer equation with a full-width-at-half-maximum (FWHM) value of 5° based on the (1 1 1) peak of the XRD pattern. TEM images of pristine CdSe and DT-capped CdSe are shown in Fig. 3; the insets show the selective area electron diffraction (SAED) patterns of the samples. Three concentric rings of SAED corresponding to (1 1 1), (2 2 0), and (3 1 1) diffraction were observed. These results are in agreement with the XRD patterns. SAED studies showed that the crystalline quality of DT-capped CdSe was not as good as that of pristine CdSe. Two factors can account for this finding. First, sulfur bonding to CdSe and second, the size of DT-capped CdSe QDs (~4 nm) was too small to obtain clear diffraction patterns.

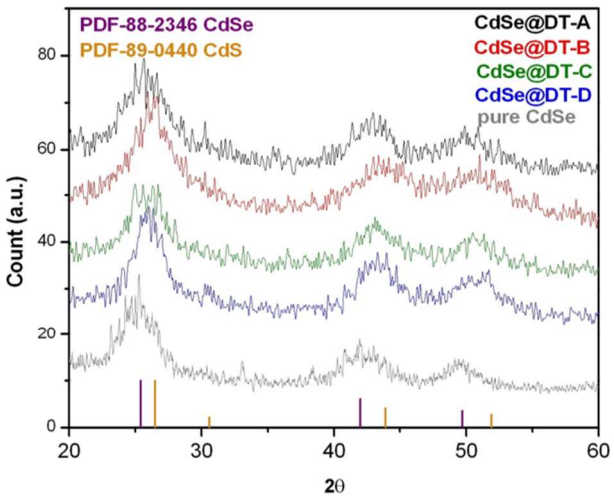

Fig. 2. XRD diffractograms of CdSe and DT-capped CdSe QDs.

TEM images of all DT-capped CdSe QDs confirmed that the QDs were spherical in shape and were highly uniform in size and shape. XRD and TEM-SAED results indicated that the CdSe quantum dots retained their crystalline structure after capping with DTs.

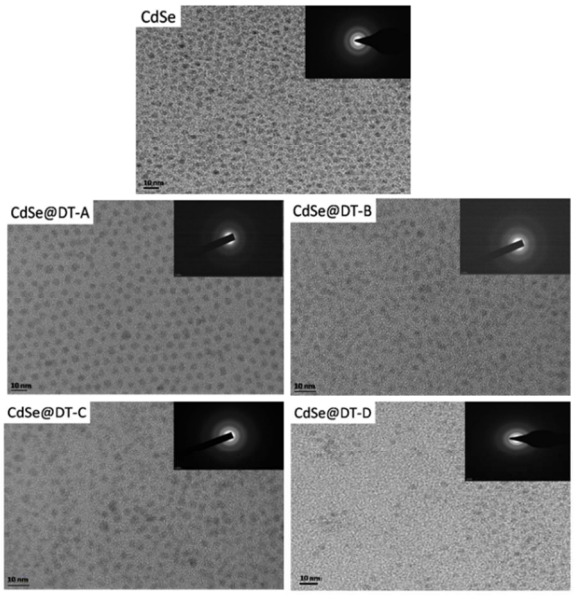

Fig. 3. TEM images of CdSe and DT-capped CdSe QDs.

Optical properties of the DT-capped CdSe QDs were investigated by UV-Vis absorption and photoluminescence (PL) spectra. Photographs of DT-capped CdSe QDs grown for four different times are presented in Fig. 4. All DT-capped CdSe QDs showed strong luminescent emission intensity under 354 nm excitation, and color emission was dependent on the size of the DT-capped CdSe QDs. We believe that the DT ligands were responsible for the strong fluorescence of the CdSe QDs. Reaction time-dependence PL emission spectra of the four DT-capped CdSe QDs are provided in Fig. 5. PL spectra of DT-capped CdSe QDs shifted towards longer wavelengths with increasing reaction time, indicating an increase in the size of the DT-capped QDs. Emission spectra shifted to the red range with increasing reaction time. Emission wavelengths varied from 494-540, 590-645, 474-574, and 490-557 nm, corresponding to

CdSe@DT-A, CdSe@DT-B, CdSe@DT-C, and CdSe@DT-D, respectively. The initial emission wavelengths of the samples are different because the DT ligands possess variant chemical activities, which affected kinetics for the creation and growth of seeds. This process will decide the shape and size of the particles to result on the different emission wavelengths. We attributed these results to extension of the exciton wave-function to the outer layer of DT ligands, resulting in a decrease in the confinement energy of excitons and wavelength red-shift. Fig. S4† show the temporal evolution time of the absorption spectra of DT-capped CdSe QDs during growth. The exciton absorption peak shifted to longer wavelengths because of an increase in the mean NCs radius with time.[42] Red-shift of the absorption spectra agreed with the red-shift of the emission wavelength, indicating an increase in QD size.

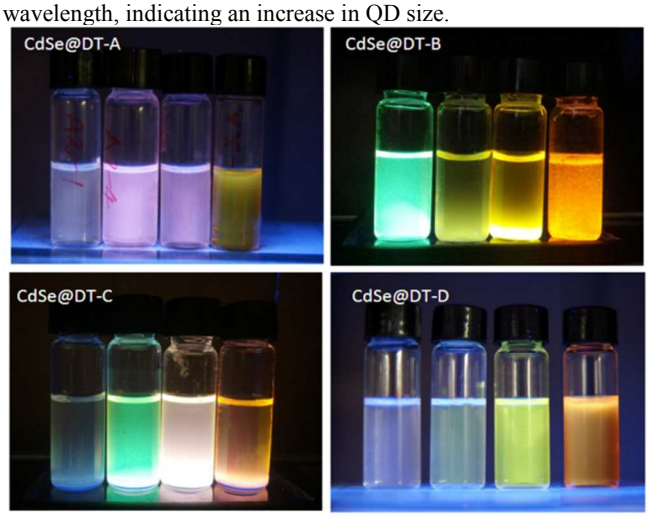

Fig. 4. Photographs of DT-capped CdSe QDs grown for four different times under 354 nm ultraviolet light excitation.

As the reaction time increased, the emission intensity of all DT-capped CdSe QDs decreased gradually. This can be explained by the fact that the DT ligands played a significant role in protecting QDs against PL by stabilizing the CdSe QDs and making them smoother by excluding surface defects. Cd bonded to sulfur atoms during synthesis, and as the reaction time increased, DT ligands formed stronger and more stable bonds and resulted in increased PL intensity. The further reaction time caused the decrease of PL intensity. The reduction of PL intensity may be originated from the low resistance to temperature of the particles. The new defects could be formed on the surface of the particles to result in the decrease of PL intensity. This decreased PL intensity indicated a non-radiative relaxation process. The reaction times for the highest PL intensity of CdSe@DT-A, CdSe@DT-B, CdSe@DT-C, and CdSe@DT-D were 1, 5, 30, and 1 min, respectively (ESI Fig.S5†). The quantum yields were determined at an excitation wavelength of 400 nm by standard procedures with an integral sphere (JASCO, ILF-533, diameter 10 cm) mounted on a spectrofluorometer (JASCO, FP-6500). The quantum yield values of CdSe, CdSe@DT-A, CdSe@DT-B, CdSe@DT-C, and CdSe@DT-D are 2.4, 11.8, 17.2, 73.5, and 21.7 %, respectively. This could be due to differences in the extent of bonding of DT ligands to CdSe QDs. In comparison to the PL intensity of different DT-capped CdSe and pure CdSe QDs, CdSe@DT-C QDs had the strongest PL intensity, as shown in ESI Fig.S5†. These differences in PL intensity suggest that the different structures and functional groups of DT ligands had different effects on the optical properties of the CdSe QDs. Although the DTs we evaluated all have two –SH groups, they have different functional groups. The different functional groups of the DTs, in particular the aromatic rings of DTs A and B, could be responsible for the reduction in CdSe emission. Theoretical calculations have shown that thiol binding to ZnS surfaces is endothermic.[43] Accordingly, we propose that bonding of DT ligands to CdSe QDs could be due to slow deprotonation of–SH groups on the QD surface, eventually resulting in binding of sulfur atoms of DTs to the CdSe shell with minimum surface modification.

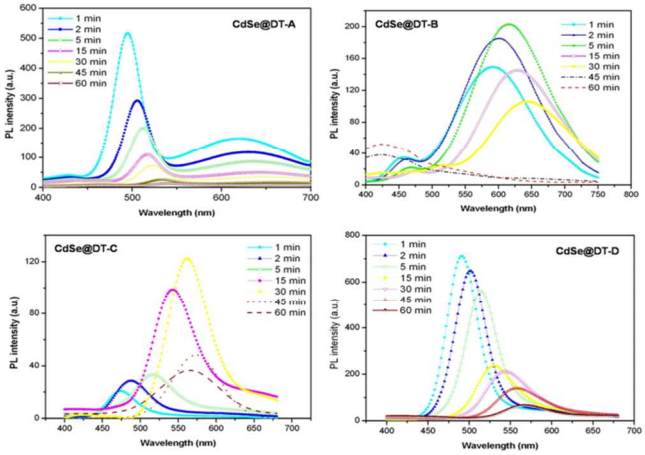

Fig. 5. PL spectra of DT-capped CdSe QDs according to reaction time.

Photocurrent density-voltage curves of QD solar cells based on DT-capped CdSe and TiO_2 are shown in ESI Fig.S6†. Table 1 summarizes the photovoltaic parameters of short-circuit current density (J_{sc}),open-circuit voltage (V_{oc}), fill factor (FF), and power .

Table 1. Detailed photovoltaic parameters of DT-capped CdSe QDSSCs.

QD	J_{SC} ($mA.cm^{-2}$)	V_{OC} (mV)	FF	η (%)
CdSe@DT-A	1.90±0.11	445±2	16.70±1.12	0.14±0.02
CdSe@DT-B	1.10±0.06	355±3	15.26±2.01	0.06±0.01
CdSe@DT-C	5.03±0.10	470±2	27.46±1.37	0.65±0.04
CdSe@DT-D	3.37±0.04	465±4	24.06±3.10	0.38±0.07

conversion efficiency (η). Efficiency ranged from 0.06 to 0.65% for the different DTs. The performance of CdSe@DT-C QDSCs was better than that of CdSe@DT-A, CdSe@DT-B, and CdSe@DT-D QDSCs.

To get inside into the dynamics of charge transport and recombination in QDSCs, electrochemical impedance spectroscopy (EIS) was accomplished under constant light illumination (100 $mWcm^{-2}$) biased in an open-circuit condition with a frequency range of 100 kHz to 100 mHz and a perturbation amplitude of 10 mV. The obtained spectra were fitted using the Z-view software (v3.2, Scribner Associate, Inc.) with reference to the proposed equivalent circuit. Fig. 6 shows the Nyquist plots of the QDSCs fabricated from different QDs. The estimated values of recombination resistance (Rct2) and electron lifetime value (τ_r) were illustrated in Table 2. As can be seen, Rct2 was decreased in the order of CdSe@DT-C, CdSe@DT-D, CdSe@DT-A and CdSe@DT-B QDSCs photoanodes, indicating the faster interfacial recombination.[44] It is known that the V_{oc} value of QDSCs was related to the charge recombination in the conduction band of TiO_2. The τ_r = Rct2 * CPE2 was used to evaluate

the difference of V_{oc} in QDSCs based on various photoanodes.[45] The τ_r of the QDSCs fabricated from CdSe@DT-C, CdSe@DT-D, CdSe@DT-A and CdSe@DT-B was 0.038, 0.025, 0.017 and 0.014 (s), respectively. It is obvious that the enhanced τ_r is strongly correlated to the increased V_{oc}, which are consistent with the results obtained from photocurrent-voltage curves.

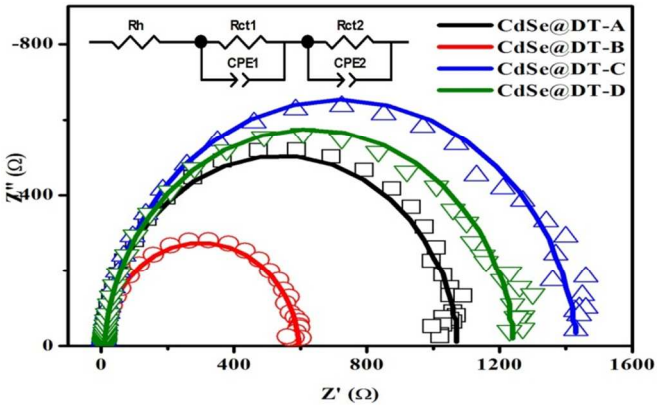

Fig. 6. Electrochemical impedance spectra of QDSCs based on different QDs in the form of Nyquist plots. The inset is the equivalent circuit applied to fit the resistance data. Rh: ohmic serial resistance; Rct1: charge-transfer resistance of counter electrode; CPE1: constant phase element of counter electrode; Rct2: charge-transfer resistance of photoanode.

Table 2. Detailed simulative value of recombination resistance (Rct2) and electron lifetime value (τ_r) from EIS spectra calculated by equivalent circuit as shown in Fig. 6.

QDSC	Rct2 (Ω)	CPE2	τ_r (s)
CdSe@DT-A	1067	1.56×10^{-5}	0.017
CdSe@DT-B	590.3	2.37×10^{-5}	0.014
CdSe@DT-C	1427	2.69×10^{-5}	0.038
CdSe@DT-D	1235	2.00×10^{-5}	0.025

Binding between CdSe@DT-C and TiO_2 likely ensured efficient charge separation as observed in the XPS analysis and TGA data. Addition of DT-capped CdSe resulted in an increased J_{sc} compared to that of pristine CdSe,[46]suggesting high photoinjection of electrons from QDs to the nanocrystalline TiO_2. The stronger coordination of DTs onto the CdSe QDs, resulting in enhanced optical properties and charge transfer between surroundings QDs, could explain this phenomenon. Additionally, CdS grown on CdSe (XPS and FT-IR analysis) co-sensitized QDSSCs for effective charge carrier transport.[47]The V_{oc} values of these devices were also higher than that of pristine CdSe.[46] This suggests the formation of a stepwise type-II band structure in CdS/CdSe/TiO_2 devices when CdS and CdSe arebrought into contact as a cascade band structure.[47]

Based on the above results, we constructed a schematic diagram of a QDSSC based on a DT-capped CdSe sensitizer; this is shown in Scheme 2. The V_{oc} of CdSe@DT-C was higher than that of the other DT-capped CdSe QDs (Table 1) due to stronger coordination of DT-C with the CdSe QDs than that other DT types, as determined by XPS analysis. The relatively low FF of QDSCs could be due to high charge transfer resistance at the counter electrode-electrolyte interface.[29] The power conversion efficiencies of CdSe@DT-C and CdSe@DT-D solar cells are higher than those reported previously.[48-51]

Conclusions

In summary, we have synthesized new DTs as novel capping ligands for CdSe QDs. The successful formation of DTs was confirmed by ^{1}H- and ^{13}C-NMR, FT-IR, and ESI-MS techniques. A direct method was utilized for capping DTs on to the surface ofCdSe QDs and their

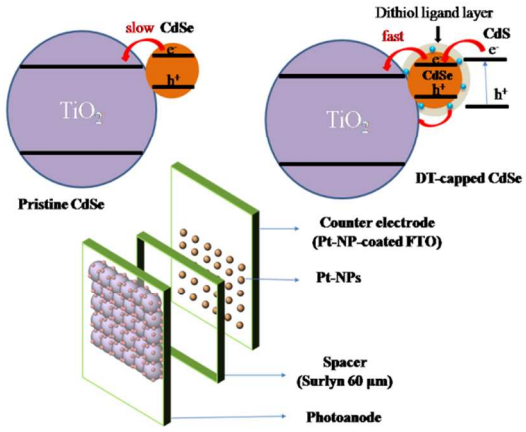

Scheme 2. Assembly of DT-capped CdSe QD solar cell andproposed electron transfer mechanism.

surface modification has been confirmed by several characterizations.XPS, FT-IR and TGA studies prove the binding of DTs to CdSe QDs. In addition, TGA reveals strong and stablebonding between CdSe and the sulfur groups of DT ligands as reflected by the higher thermal stabilities of DT-capped CdSe QDs than pureCdSeQDs.TEMcharacterization exposesall DT-capped CdSe QDs were spherical in shape (~4 nm) and were highly uniform in size and shape. XRD and TEM-SAED results indicated that the CdSe quantum dots retained their crystalline structure after capping with DTs.All DT-capped CdSe QDs showed strong luminescent emission intensity, and color emission was dependent on the size of the DT-capped CdSe QDs. It has been believed that the DT ligands were responsible for the strong fluorescence of the CdSe QDs. The difference in PL intensity of DT-capped CdSe QDs was proposed to be due to different structures and functional groups of DT ligands had different effects on the optical properties of the CdSe QDs. We have also demonstrated the promising use of the new DT-capped CdSe QDs in solar cells application. The synthetic strategy holds promise in the preparation of functional ligands and their capping onto different QDs for significant applications in future.

Experimental

Reagents and Chemicals

Cadmium oxide (CdO, 99.99%), selenium (Se, 99.9%), 1-octadecene (ODE, 90%), and oleic acid (OA, 90%) were purchased from Aldrich. $H_2PtCl_6.xH_2O$ (≥37.5% Pt), isopropanol, and hexane (analytical grade) were obtained from Sigma-Aldrich. Acetone was obtained from Fluka. TiO_2 (P25), 2 M Na_2S, and 2 M sulfur to prepare the electrolyte for solar cell applications were supplied by Sigma-Aldrich. Chemicals used to synthesize dithiols are commercially available. All reagents were used as received without further purification.

Characterization techniques

^{1}H-and ^{13}C-NMR spectra of synthesized DTs were recorded using a Bruker Avance-400 spectrometer. Fourier transform infrared (FT-

IR) spectra were recorded on a JASCO 6300 FT-IR spectrometer (Japan). Mass spectrometry (MS) data of DTs were obtained using a LCQ-Fleet (Thermo Fisher, USA) ion trap mass spectrometer equipped with an ESI source.Morphology of DT-capped CdSe QD samples was determined using a JEM-2100F transmission electron microscope (TEM) (JEOL, Japan) operating at an acceleration voltage of 200 kV. X-ray diffraction (XRD) patterns were measured using X-ray diffraction (Philips X'pert MPD 3040) with Cu Kα radiation over the 2θrange of 20^{o}to 60^o. X-ray photoelectron scanning microscopy (XPS) of DT-capped CdSe QDs was performed using an ESCALAB250 instrument (VG Scientific Company, USA) with Al Kα radiation as the excitation source. Thermal gravimetric analysis (TGA) was performed on a Mettler-Toledo International Inc. (Switzerland) instrument under N_2 gas flow. UV-Vis absorption and fluorescence spectra were recorded at room temperature using a UV-Vis spectrophotometer Agilent 8543 (Agilent, US) and spectrofluorometer FP-6500 (Jasco, Japan), respectively. Photocurrent-voltage characteristics were measured with an IVIUMSTAT under illumination from a Sun 3000 solar simulator composed of 1000 W mercury-based Xe arc lamps and AM 1.5 G filters. Light intensity was calibrated with a silicon photodiode.

Synthesis of dithios (DTs)

Synthesis of DTs is presented in Scheme S5. Briefly, amine (0.9 g, 0.01 mol) was added to a THF solution of cyanuric chloride (2 g, 0.01 mol) at -5^{o}C to 0^{o}C over a period of 30 min. Aqueous Na_2CO_3 (0.57 g, 0.005 mol) was added over a period of 30 min at the same temperature and stirred for 30 min. The mixture was then treated with aqueous NaSH (1.12 g, 0.02 mol) under stirring at 50^{o}C over a period of 10 min and stirring was continued at 50^{o}C for 30 min. Then, the reaction mixture was acidified with 5% HCl and worked-up with ethyl acetate; the organic layer that formed was washed with water and dried over Na_2SO_4. The organic layer was concentrated to give corresponding DTs with a greater than 70% yield.

DT-A: Light whitish brown solid, melting point: 243–245^{o}C. ^{1}H-NMR (400 MHz, acetone-d_6): δ 10.36 (bs, 2H), 8.13 (d, J = 7.32 Hz, 2H), 7.53 (dt, J = 7.32, 8.33 Hz, 2H), 7.4 (dd, J = 7.32, 8.32 Hz, 2H), 7.19 (dd, J = 7.32, 8.08 Hz, 2H). ^{13}C-NMR (100 MHz, DMSO-d$_6$): δ 177.0, 150.0, 139.9, 125.3, 122.7, 119.8, 118.5, 110.8. ESI-MS: *m/z* 332.86 ([M+Na]$^+$). FT-IR (KBr) (υ cm^{-1}): 3045 (aromatic C-H), 2575 (S-H), 1545 (aromatic C=C), 1235 (C-N), 725 (C-S).

DT-B: Light yellowish green solid, melting point: 105–107^{o}C. ^{1}H-NMR (400 MHz, DMSO-d_6): δ 10.68 (bs, 2H), 7.14 – 7.5 (m, 10H), 4.67 – 5.06 (m, 4H). ^{13}C-NMR (100 MHz, DMSO-d$_6$): δ 175.7, 159.8, 136.0, 128.4, 127.2, 127.0, 56.4. ESI-MS:*m/z* 362.92 ([M+Na]$^+$). FT-IR (KBr) (υ cm^{-1}): 3034 (aromatic C-H), 2579 (S-H), 1588 (aromatic C=C), 1134 (C-N), 731 (C-S).

DT-C: Light yellowish green solid, melting point: 185–187^{o}C. ^{1}H-NMR (400 MHz, DMSO-d_6): δ 10.63 (bs, 2H), 3.47 – 3.85 (m, 8H). ^{13}C-NMR (100 MHz, DMSO-d$_6$): δ 163.9, 153.1, 65.4, 44.8. ESI-MS: *m/z* 252.17 ([M+Na]$^+$). FT-IR (KBr) (υ cm^{-1}): 3031 (aromatic C-H), 2568 (S-H), 1592 (aromatic C=C), 1265 (C-N), 1040 & 1097 (C-O-C), 743 (C-S).

DT-D (400 MHz, DMSO-d_6):Light yellowish green solid, melting point: 214–216^{o}C. ^{1}H-NMR: δ 7.76 (s, 2H), 3.41 – 3.57 (m, 4H), 1.86 – 1.98 (m, 4H). ^{13}C-NMR (100 MHz, DMSO-d$_6$): δ 168.4, 162.1, 47.0, 24.4. ESI-MS: *m/z* 236.08 ([M+Na]$^+$). FT-IR (KBr) (υ cm^{-1}): 3037 (aromatic C-H), 2572 (S-H), 1612 (aromatic C=C), 1131 (C-N), 748 (C-S).

Synthesis of DT-capped CdSe QDs

Selenium solution was prepared by dissolving selenium powder (16.2 mg) in ODE (2 mL) at 200^{o}C until the solution turned colorless. Subsequently, the DT solution in acetone was mixed with the selenium solution at 70^{o}C. This mixture was used as the Se precursor solution. Cadmium precursor solution was prepared by heating a mixture of CdO (15.2 mg), OA (105 mg), and ODE (10 mL) to 290^{o}C until the solution became optically clear and colorless. At this point, the selenium precursor solution was quickly injected and the temperature was stabilized at 260^{o}C for NC growth. Reaction times ranging from 30 sec to 1 hour were investigated. NCs were isolated from the growth solution by precipitation with 2-isopropanol, followed by repeated hexane/2-isopropanol extractions. The reference sample was prepared using the same procedure except that DT was absent from the selenium precursor solution.

Preparations of Pt counter electrodes

Pt counter electrodes were prepared by dry plasma reduction as per the reported method.[52] Briefly, a Pt precursor solution containing 10 mM $H_2PtCl_6.XH_2O$ in isopropanol was first prepared. An 8 µl aliquot of Pt precursor solution was deposited on 2 cm x 2 cm square specimens of FTO glass (~8 Ω /cm^2, Pilkington, USA), and solvent was allowed to evaporate at 70 ^{o}C for about 10 min. Specimens were then reduced using Argon (Ar) plasma under atmospheric pressure at a power of 150 W, gas flow rate of 5 lpm, treatment time of 15 min, and substrate moving speed of 5 mm/s.

Preparations of TiO_2 working electrodes

We fabricated DT-capped CdSe quantum dot solar cell (QDSC) working electrodes coated with a TiO_2 layer of 0.7 cm x 0.7 cm on FTO glass (2 cm x 2 cm) using the following procedure.[53] Substrates were first cleaned using acetone in an ultrasonic bath for 30 min. After cleaning, substrates were immersed in 40 mM aqueous $TiCl_4$ solution at 70 ^{o}C for 30 min and washed with water and ethanol, respectively. A transparent film of 20 nm TiO_2 particles (Solaronix, Switzerland) was coated on the substrates by screen printing (200 T mesh), kept in a clean box for 3 min so that the paste could relax to reduce surface irregularities, and then dried for 3 min at 125 ^{o}C. This screen-printing procedure (coating, storing, and drying) was repeated till the thickness of the working electrode was around 12 µm. We then also coated a 4 µm-thick scattering layer of TiO_2 paste (DSL 18 NR-AO, Dyesol-Timo, Australia) on a working electrode. Electrodes coated with TiO_2 paste were gradually heated under air flow at 325 ^{o}C for 5 min, at 375 ^{o}C for 5 min, at 450^{o}C for 15 min, and finally at 500^{o}C for 15 min under ambient conditions. After annealing, TiO_2 film was treated with 40 mM $TiCl_4$ solution as described above, and then sintered at 500 ^{o}C for 30 min.[53] After cooling down to room temperature, TiO_2 electrodes were immersed in DT-capped CdSe quantum dot solution in toluene and kept at room temperature for 5 days to complete sensitizer uptake.[54]

Assembly of DT-capped CdSe QDs for solar cell application

DT-capped CdSe QD-covered TiO_2 electrode and a Pt-counter electrode were assembled onto a sandwich type cell and sealed at 120 ^{o}C/5 min with a thermobonding polymer (Surlyn, DuPont) of 60 µm thickness.[52, 53] A drop of polysulfide electrolyte, a solution of 2 M Na_2S and 2 M sulfur in aqueous solution, was placed on the holes (0.8 mm) in the back of the working electrode.[55] Holes were sealed with a Surlyn layer.[52, 53]

Acknowledgements

This work was supported by the Regional University Research Program (NRF2014-008793) and the Priority Research Centers Program (NRF 2010-0029634), through the National Research Foundation of Korea (NRF) funded by the Ministry of Education, Science and Technology.

References

1. P. V. Kamat, *J. Phys. Chem. Lett*, 2013, **4**, 908-918.
2. M. Nurunnabi, Z. Khatun, M. Nafiujjaman, D.-g. Lee and Y.-k. Lee, *ACS Appl. Mater. Interfaces*, 2013, **5**, 8246-8253.
3. L. Qian, J. Yang, R. Zhou, A. Tang, Y. Zheng, T.-K. Tseng, D. Bera, J. Xue and P. H. Holloway, *J. Mater. Chem.*, 2011, **21**, 3814-3817.
4. J. Zhao, J. A. Bardecker, A. M. Munro, M. S. Liu, Y. Niu, I. K. Ding, J. Luo, B. Chen, A. K. Y. Jen and D. S. Ginger, *Nano Lett.*, 2006, **6**, 463-467.
5. V. I. Klimov, A. A. Mikhailovsky, S. Xu, A. Malko, J. A. Hollingsworth, C. A. Leatherdale, H.-J. Eisler and M. G. Bawendi, *Science*, 2000, **290**, 314-317.
6. P. V. Kamat, K. Tvrdy, D. R. Baker and J. G. Radich, *Chem. Rev. (Washington, DC, U. S.)*, 2010, **110**, 6664-6688.
7. J. H. Bang and P. V. Kamat, *ACS Nano*, 2009, **3**, 1467-1476.
8. J. Wei, C. Zhang, Z. Du, H. Li and W. Zou, *J. Mater. Chem. C*, 2014, **2**, 4177-4185.
9. W. W. Yu, L. Qu, W. Guo and X. Peng, *Chem. Mater.*, 2003, **15**, 2854-2860.
10. D. J. Norris and M. G. Bawendi, *Phys. Rev. B: Condens. Matter Mater. Phys.*, 1996, **53**, 16338-16346.
11. P. Yu, X. Wen, Y.-R. Toh, Y.-C. Lee, K.-Y. Huang, S. Huang, S. Shrestha, G. Conibeer and J. Tang, *J. Mater. Chem. C*, 2014, **2**, 2894-2901.
12. N. C. Greenham, X. Peng and A. P. Alivisatos, *Phys. Rev. B: Condens. Matter Mater. Phys.*, 1996, **54**, 17628-17637.
13. K. F. Jeltsch, M. Schädel, J.-B. Bonekamp, P. Niyamakom, F. Rauscher, H. W. A. Lademann, I. Dumsch, S. Allard, U. Scherf and K. Meerholz, *Adv. Funct. Mater.*, 2012, **22**, 397-404.
14. R. Zhou, Y. Zheng, L. Qian, Y. Yang, P. H. Holloway and J. Xue, *Nanoscale*, 2012, **4**, 3507-3514.
15. M. Wright and A. Uddin, *Sol. Energy Mater. Sol. Cells*, 2012, **107**, 87-111.
16. N. T. N. Truong, W. K. Kim, U. Farva, X. D. Luo and C. Park, *Sol. Energy Mater. Sol. Cells*, 2011, **95**, 3009-3014.
17. S. N. Sharma, T. Vats, N. Dhenadhayalan, P. Ramamurthy and A. K. Narula, *Sol. Energy Mater. Sol. Cells*, 2012, **100**, 6-15.
18. H. Skaff and T. Emrick, *Chem. Commun. (Cambridge, U. K.)*, 2003, 52-53.
19. M.-Q. Zhu, E. Chang, J. Sun and R. A. Drezek, *J. Mater. Chem.*, 2007, **17**, 800-805.
20. Y. A. Wang, J. J. Li, H. Chen and X. Peng, *J. Am. Chem. Soc.*, 2002, **124**, 2293-2298.
21. Y. Liu, M. Kim, Y. Wang, Y. A. Wang and X. Peng, *Langmuir*, 2006, **22**, 6341-6345.
22. J. Seo, W. J. Kim, S. J. Kim, K.-S. Lee, A. N. Cartwright and P. N. Prasad, *Appl. Phys. Lett.*, 2009, **94**, -.
23. Y. Peng, G. Song, X. Hu, G. He, Z. Chen, X. Xu and J. Hu, *Nanoscale Res. Lett.*, 2013, **8**, 106.
24. D. H. Webber and R. L. Brutchey, *J. Am. Chem. Soc.*, 2011, **134**, 1085-1092.
25. I. S. Liu, H.-H. Lo, C.-T. Chien, Y.-Y. Lin, C.-W. Chen, Y.-F. Chen, W.-F. Su and S.-C. Liou, *J. Mater. Chem.*, 2008, **18**, 675-682.
26. M. Soreni-Harari, N. Yaacobi-Gross, D. Steiner, A. Aharoni, U. Banin, O. Millo and N. Tessler, *Nano Lett.*, 2008, **8**, 678-684.
27. D. V. Talapin, A. L. Rogach, A. Kornowski, M. Haase and H. Weller, *Nano Lett.*, 2001, **1**, 207-211.
28. C. Bullen and P. Mulvaney, *Langmuir*, 2006, **22**, 3007-3013.
29. K. M. Coughlin, J. S. Nevins and D. F. Watson, *ACS Appl. Mater. Interfaces*, 2013, **5**, 8649-8654.
30. Z. Pan, K. Zhao, J. Wang, H. Zhang, Y. Feng and X. Zhong, *ACS Nano*, 2013, **7**, 5215-5222.
31. I. Yildiz, E. Deniz, B. McCaughan, S. F. Cruickshank, J. F. Callan and F. i. M. Raymo, *Langmuir*, 2010, **26**, 11503-11511.
32. M. H. Stewart, K. Susumu, B. C. Mei, I. L. Medintz, J. B. Delehanty, J. B. Blanco-Canosa, P. E. Dawson and H. Mattoussi, *J. Am. Chem. Soc.*, 2010, **132**, 9804-9813.
33. G. Palui, H. B. Na and H. Mattoussi, *Langmuir*, 2011, **28**, 2761-2772.
34. Y. Chen, R. Thakar and P. T. Snee, *J. Am. Chem. Soc.*, 2008, **130**, 3744-3745.
35. A. Lobo, T. Möller, M. Nagel, H. Borchert, S. G. Hickey and H. Weller, *J. Phys. Chem. B*, 2005, **109**, 17422-17428.
36. C. Vargas-Hernández, V. C. Lara, J. E. Vallejo, J. F. Jurado and O. Giraldo, *Phys. Status Solidi B*, 2005, **242**, 1897-1901.
37. M. Polak, *J. Electron Spectrosc. Relat. Phenom.*, 1982, **28**, 171-176.
38. J. E. B. Katari, V. L. Colvin and A. P. Alivisatos, *J. Phys. Chem.*, 1994, **98**, 4109-4117.
39. M. Ichimura, K. Takeuchi, A. Nakamura and E. Arai, *Thin Solid Films*, 2001, **384**, 157-159.
40. B. T. Huy, M.-H. Seo, A. P. Kumar, H. Jeong and Y.-I. Lee, *J. Alloys Compd.*, 2014, **588**, 127-132.
41. A. G. Young, D. P. Green and A. J. McQuillan, *Langmuir*, 2006, **22**, 11106-11112.
42. G. G. Yordanov, E. Adachi and C. D. Dushkin, *Colloids Surf., A*, 2006, **289**, 118-125.
43. B.-K. Pong, B. L. Trout and J.-Y. Lee, *Langmuir*, 2008, **24**, 5270-5276.
44. R. Zhou, Q. Zhang, E. Uchaker, J. Lan, M. Yin and G. Cao, *J. Mater. Chem. A*, 2014, **2**, 2517-2525.
45. W.-Q. Wu, Y.-F. Xu, C.-Y. Su and D.-B. Kuang, *Energy & Environmental Science*, 2014, **7**, 644-649.
46. T. Yang, M. Lu, X. Mao, W. Liu, L. Wan, S. Miao and J. Xu, *Chem. Eng. J. (Lausanne)*, 2013, **225**, 776-783.
47. M. Seol, H. Kim, Y. Tak and K. Yong, *Chem. Commun. (Cambridge, U. K.)*, 2010, **46**, 5521-5523.
48. Y.-L. Xie, *Electrochim. Acta*, 2013, **105**, 137-141.
49. S. A. Pawar, R. S. Devan, D. S. Patil, A. V. Moholkar, M. G. Gang, Y.-R. Ma, J. H. Kim and P. S. Patil, *Electrochim. Acta*, 2013, **98**, 244-254.
50. X. Xu, S. Giménez, I. Mora-Seró, A. Abate, J. Bisquert and G. Xu, *Mater. Chem. Phys.*, 2010, **124**, 709-712.
51. J. Wang, T. Zhang, D. Wang, R. Pan, Q. Wang and H. Xia, *Chem. Phys. Lett.*, 2012, **541**, 105-109.
52. V.-D. Dao, C. Q. Tran, S.-H. Ko and H.-S. Choi, *J. Mater. Chem. A*, 2013, **1**, 4436-4443.
53. V.-D. Dao, S.-H. Kim, H.-S. Choi, J.-H. Kim, H.-O. Park and J.-K. Lee, *J. Phys. Chem. C*, 2011, **115**, 25529-25534.
54. A. Kongkanand, K. Tvrdy, K. Takechi, M. Kuno and P. V. Kamat, *J. Am. Chem. Soc.*, 2008, **130**, 4007-4015.

55. Q. Zhang, Y. Zhang, S. Huang, X. Huang, Y. Luo, Q. Meng and D. Li, *Electrochem. Commun.*, 2010, **12**, 327-330.

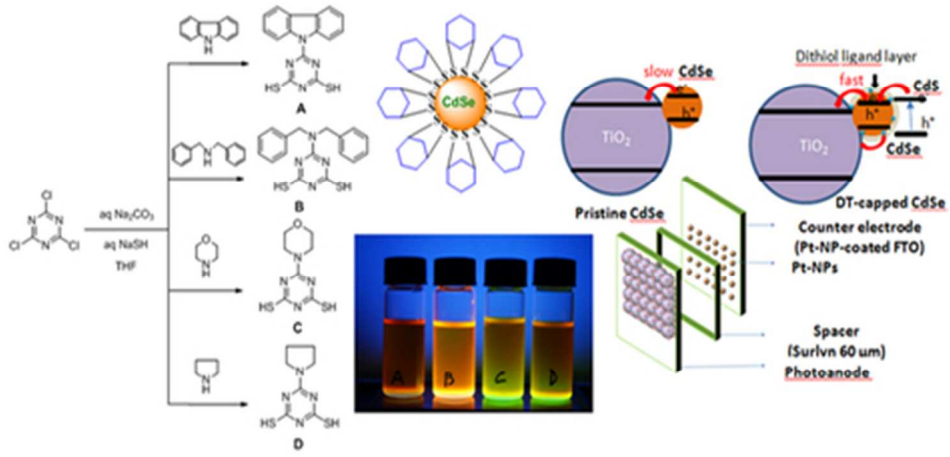

39x19mm (300 x 300 DPI)